Supporting Information

High throughput discovery of complex metal oxide electrocatalysts for the oxygen reduction reaction

Dan Guevarra, Joel A. Haber, Yu Wang, Lan Zhou, Kevin Kan, Matthias H. Richter, John M. Gregoire

Figure S1 provides a summary of non-transition metal modification of the activity of transition metal oxides. As noted in the manuscript, the transition metal oxides provide most of the catalytic activity, and to survey the many composition spaces of the high throughput campaign, we consider the propensity for additional non-transition metal elements to increase or decrease activity. In the figure, $x = 0$ corresponds to the set of catalyst compositions with any combination of Mn, Ni, and Fe with no additional elements. Upon adding 10%-20% of an additional element, only Mg and Ca increase the median activity, and for higher concentrations, the general trend is decreasing activity with decreasing concentration of the transition metal concentration.

Note on reporting of electrochemical potential: Our Ag/AgCl reference electrodes are 2.0 M KCl and are calibrated against a commercial BASi Ag/AgCl reference electrode stored in 3.0M NaCl. A 12 mV offset is added to the reference calibration to account for the difference in Cl- concentrations. The reference electrode potential versus RHE was calculated for the 1.0 M NaOH working electrolyte using pH values measured by pH meter at room temperature.

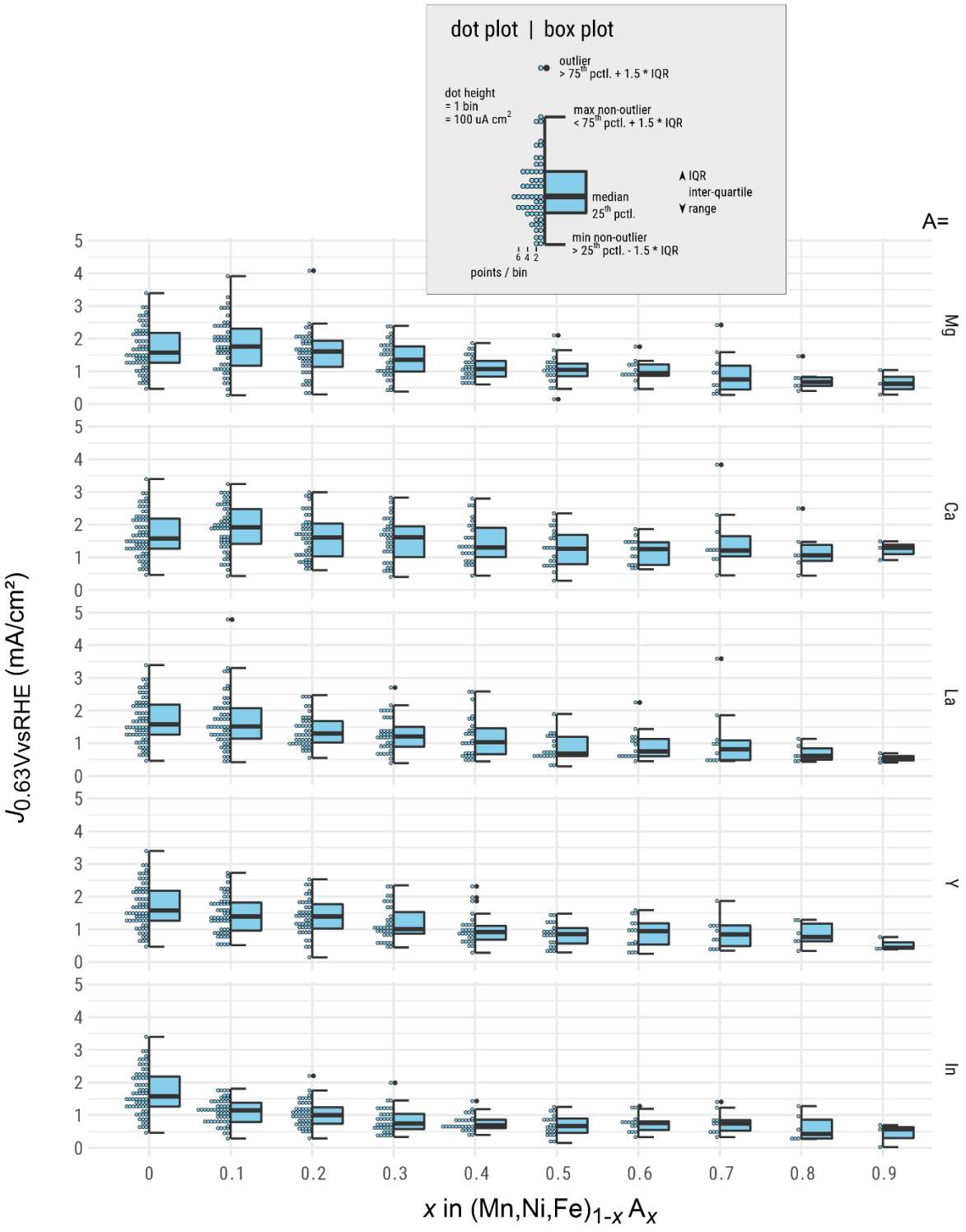

Figure S1: Summary of non-transition metal modification of the activity of transition metal oxides. For each of the 5 non-transition metal elements (A = Mg, Ca, La, Y, In) and each of their concentrations with respect to the sum of the transition metals (x = 0, 0.1, …, 0.9), the figure contains a hybrid dot-box plot that provides information on the distribution of the activities as well as statistics such as the median and interquartile range.

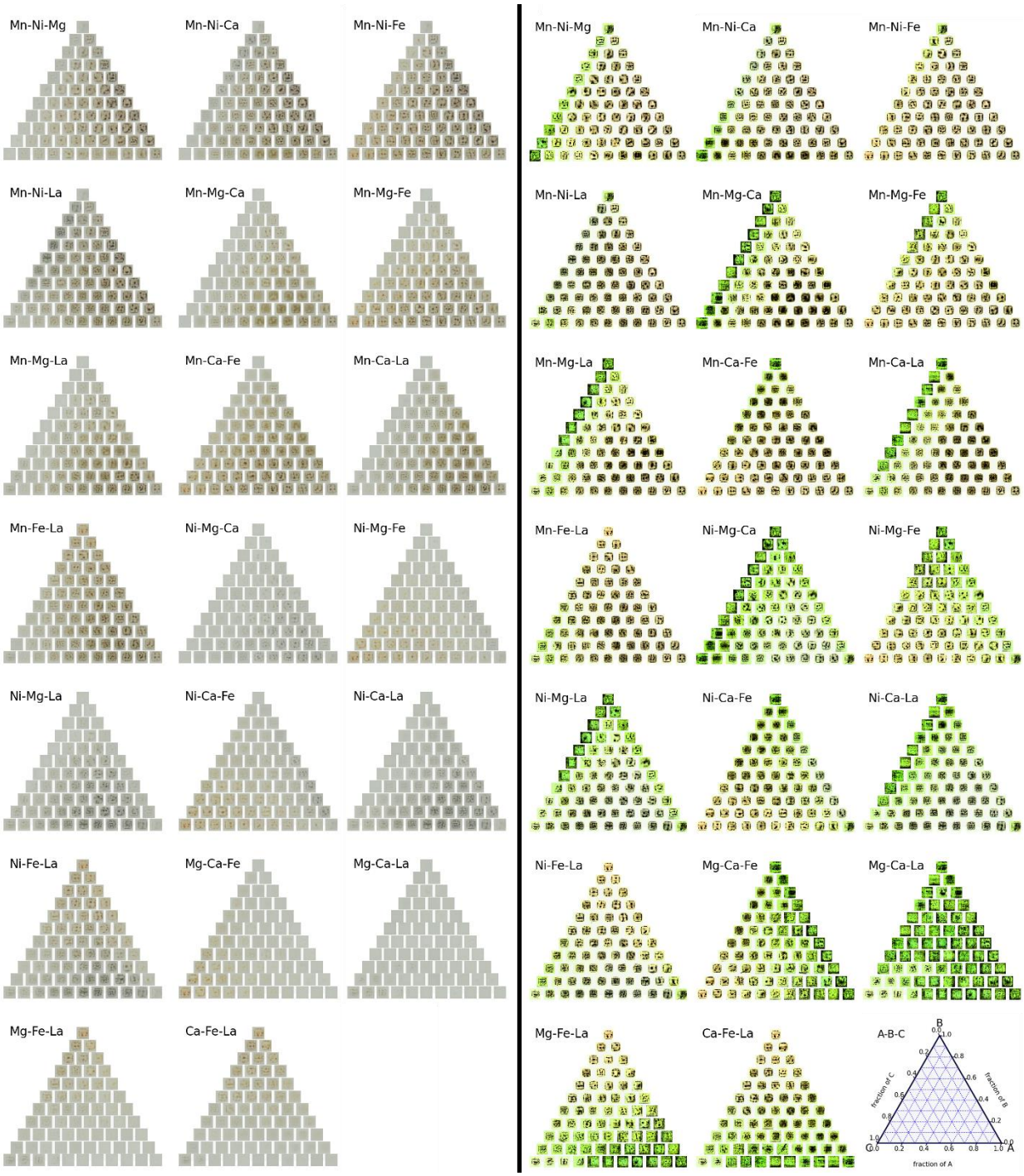

Figure S2: Mn-Ni-Mg-Ca-Fe-La oxide samples was digitally imaged at 1200 dpi using an Epson document scanner. Each of the 20 3-cation combinations of these elements is shown as a triangle composition plot reconstructed from 1×1 mm^2 images of the printed samples. The left-hand side contains the raw images from the scanner and the right-hand side contains modified versions that enhance the contrast (especially for high transparency samples like Ca and Mg) by rescaling using a min value as the 5^{th} percentile and max value as the 95^{th} percentile for each channel, followed by exposure equalization.

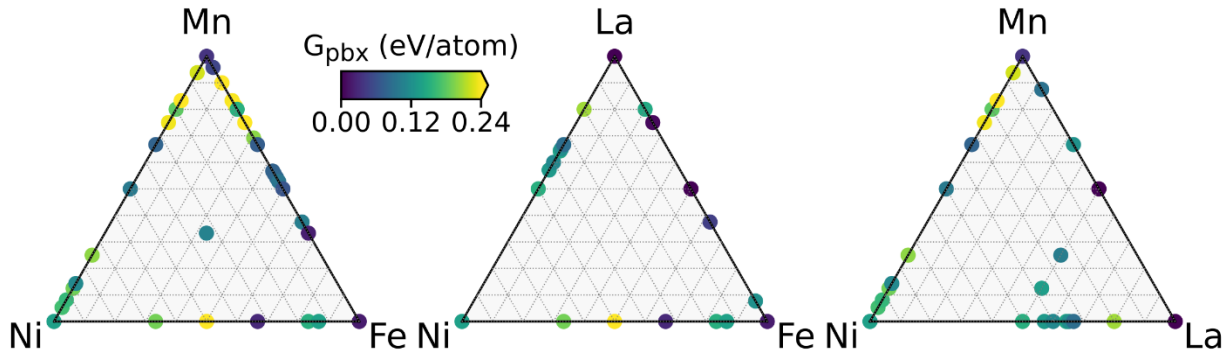

Figure S3: At pH 14 and 0.63 V vs RHE, the energy about the Pourbaix hull for known phases at various cation compositions is shown (elemental ionic concentration 10^{-8} M). Each point corresponds to a different metal oxide formula and is colored by the minimum energy above hull for all known phases at that cation composition. This analysis shows that all 2-cation composition systems contain known phases that are near or on the Pourbaix hull.

Table S1: The Materials Project entries corresponding to Fig. S3. For each material, the solid state energy above hull is shown to assess the contribution to the Pourbaix energy above hull from the solid state energy above hull. The Pourbaix energy above hull is at 0.63 V vs RHE, pH 14, and 1e-8 M elemental aqueous concentration.

material_id	pretty_formula	Energy above hull (eV/atom)		material_id	pretty_formula	Energy above hull (eV/atom)	
		Solid state	Pourbaix			Solid state	Pourbaix
mp-1172875	Mn2O3	0.000	0.036	mp-35596	Fe2NiO4	0.000	0.028
mp-19009	NiO	0.000	0.135	mp-1225019	Fe5NiO8	0.089	0.151
mp-19770	Fe2O3	0.000	0.018	mp-757258	Fe13(NiO10)2	0.067	0.137
mp-2292	La2O3	0.000	0.000	mp-574915	LaFe12O19	0.088	0.121
mp-757698	Mn23FeO32	0.014	0.050	mp-1189182	LaMn7O12	0.064	0.091
mp-753618	Mn9FeO10	0.035	0.249	mp-21444	LaMn2O5	0.083	0.122
mp-755276	Mn5FeO12	0.064	0.237	mp-1223093	La4Mn(NiO4)3	0.026	0.134
mp-771188	Mn13Fe3O32	0.080	0.256	mp-1188812	La2MnNiO6	0.042	0.101
mp-754261	La4FeO8	0.086	0.144	mp-531717	La5Mn5O16	0.000	0.000
mp-757061	Mn4FeO8	0.093	0.152	mp-1076121	La2Ni2O5	0.091	0.151
mp-1180667	La3FeO6	0.005	0.005	mp-558316	La4Ni3O10	0.020	0.129
mp-756788	Mn3FeO8	0.067	0.250	mp-18926	La3Ni2O7	0.023	0.112
mp-769622	Mn9(FeO6)4	0.081	0.198	mp-757549	La9Ni5O19	0.084	0.140
mp-1221897	MnFeNiO4	0.060	0.105	mp-1178158	La15(NiO4)8	0.049	0.117
mp-754642	Mn2FeO4	0.042	0.071	mp-21874	La2NiO4	0.047	0.086
mp-640147	Fe(NiO2)2	0.010	0.189	mp-510747	La4NiO8	0.087	0.206
mp-532236	Mn17Fe13O40	0.050	0.076	mp-758680	Mn(Ni9O10)2	0.041	0.168
mp-1222437	Mn5(FeO3)4	0.050	0.076	mp-758834	Mn3(Ni17O20)2	0.037	0.160
mp-762538	Mn13Fe11O32	0.053	0.079	mp-1221343	MnNi7O8	0.045	0.188
mp-706492	Mn19Fe17O48	0.068	0.094	mp-19442	Mn(Ni3O4)2	0.000	0.113
mp-1078634	LaFeO3	0.000	0.000	mp-759859	MnNi3O4	0.049	0.199
mp-674482	MnFeO3	0.036	0.063	mp-19331	MnNiO3	0.000	0.098
mp-1276430	FeNiO3	0.078	0.275	mp-36843	Mn2NiO4	0.012	0.076
mp-1212003	La3Fe5O12	0.040	0.044	mp-776651	Mn3NiO4	0.052	0.235
mp-757662	Mn3Fe5O12	0.077	0.102	mp-757060	Mn4NiO8	0.093	0.180
mp-18750	Mn(FeO2)2	0.000	0.020				